

## Fabrication Of Novel Metal-Free Phosphorous Doped Boron Nitride As UV-Active Photo-Catalyst

Shinwar A. Idrees<sup>a\*</sup>, Lazgin A. Jamil<sup>a</sup>, Khalid M. Omer<sup>b</sup>

*a) Department of Chemistry, Faculty of Science, University of Zakho, Kurdistan Region, Iraq*

*b) Department of Chemistry, Faculty of Science, University of Sulaimani, Kurdistan Region, Iraq*

Received 10 October 2021; received in revised form 20 December 2021; accepted 26 December 2021

### ABSTRACT

The goal of this research is to create nanostructured metal free phosphorous doped Boron nitride (P-BN) and phosphorous-carbon co-doped Boron nitride (CP-BN) that serve as photocatalysts when exposed to UV light. P-NPs were well diffused in aqueous solution. The nanostructured materials were characterized using XRD, SEM-EDX, and UV-Vis spectrophotometry. Based on the characterization results, phosphorous atoms were doped in the crystal structure of BN. The experimental data and theoretical calculations were used to measure the band gap energy, which was determined to be around 4.2 eV in the experimental case; for this purpose, both Tauc and Kubelka-Munk equations were utilized. Thus, photocatalysis degradation is limited to UV region. To examine the degradation effectiveness of photo-catalysts, toluidine blue (TB) was utilized; it was found that the basic medium was the best for degradation; 16% and 8% of TB were eliminated with CP-BN and P-BN, respectively after one hour degradation. Scavengers such as IPA, Na<sub>2</sub>C<sub>2</sub>O<sub>4</sub>, KBrO<sub>3</sub>, and ascorbic acid were added to trapping experiments to demonstrate the correct potential energy gap in valance and conduction bands and possible photocatalytic mechanism. Data from trapping experiments show that both the hydroxyl radical and super oxide are responsible for degradation, but electron and hole at valance and conduction bands were of low efficiency because of quick recombination. As regards computational study, the crystal and electronic structures of the P-BN and CP-BN have been studied. The lattice parameters were calculated with the Perdew-Burke-Ernzerhof (PBE), and the bandgaps (E<sub>g</sub>) were calculated with the (PBE) as (non-local) instead of local (non-local functional generalized gradient approximations) (GGA). In addition, hybrid functional was also applied including (Becke-3 Parameter-Lee-Yang-Parr) B3LYP and (Heyd-Scuseria-Ernzerhof) exchange-correlation functional HSE06. Hybrid functional B3LYP provided better results and closer to the experimental data of the P-BN and CP-BN compound.

**Keywords:** *Phosphorous doped boron nitride, Scavengers trapping experiment, Photo-catalysts and Photo degradation.*

### 1. Introduction

The release of harmful and pervasive organic contaminants into water bodies and the atmosphere has been a source of concern for modern social orders. Pesticides, synthetic textile colors, and industrial dyes are examples of manufactured compounds that are harmful to the environment. These pollutants cause serious damages to the ambient atmosphere. Furthermore, most drugs, pesticides, and dye molecules have an aromatic structure in their shape, which is highly toxic, carcinogenic, mutagenic, and affects the

immune system [1]. Degradation of molecules refers to the cleavage of new bonds in a molecular structure to convert a hazardous substance into a nontoxic one, or to break down to its main constituents such as water, carbon dioxide, and so on, through a process known as mineralization. Different physical, chemical, and biological procedures have been widely used to address wastewater contamination, but each strategy has its own set of drawbacks[2-5]. Phosphorus doped boron nitride and carbon phosphorous co-doped boron nitride were prepared in this research, then the nanostructured that had been created were characterized. It was discovered that the manufactured photo-catalyst has a band gap energy of about 4.2 eV and is UV active photocatalyst.

\*Corresponding author:

E-mail address: [shinwar.idrees@uoz.edu.krd](mailto:shinwar.idrees@uoz.edu.krd) (S. A. Idrees)

Boron nitride (BN) is commonly used; hexagonal boron nitride (BN) nanomaterials, with a broad specific surface area, bear negatively charged properties, high thermal conductivity; and chemical stability characteristics have major benefits for waste water treatment and power storage two-dimensional metal-free substance with a shape that has been similar to graphite [6]. BN has many typical graphite characteristics, including anisotropy, perpendicularity of the base plane, high hardness, heat capacity, and reasonable lubricity [7]. Moreover, the special structural features of the interlayer packing layout of BN, unlike graphite, give it several extra electrical, optical, and chemical properties. These characteristics make BN very useful for countless applications[8], [9]. Using similar amounts of boron (B) and nitrogen (N) atoms, boron nitrides (BN) are built. They have three isoelectronic crystalline forms of equally formed carbon lattices: hexagonal graphite-like BN (h-BN), cubic diamond-like BN (c-BN), and wurtzite BN (w-BN), BN is indeed present in the modes of sp<sup>2</sup>-bonded rhombohedra and hexagonal BN, close to carbon (hBN) [10]. The polarity of B-N bonds is indicated by such structural features, in other words, the partly ionic nature of the B-N covalent bonds, because of their greater electronegativity and electron pairs in sp<sup>2</sup>-hybridized B-N s bonds, seems to be more restricted to the N atoms; and the lone pair of electrons in the N p<sub>z</sub> orbital has only been partially delocalized with the B p<sub>z</sub> orbital, in comparison to the similarly allocated and uniformly distributed electrons all along with graphite sheet C-C bonds [7]. In addition, h-BN has attracted increasing attention recently due to the diverse functionalities such as strong deep UV luminescence and field emission properties which give great potential for a wide application in advanced technologies [11].

BN has been fabricated in various nanomaterials, which include standard zero-dimensional (0D) fullerenes and nanomaterials are geometric analogs to C<sub>60</sub> Bucky balls, one-dimensional (1D) nanotubes and nano ribbons, two-dimensional (2D) Nanosheets and three-dimensional (3D) non-porous BNN sheets [9]. Porous BNs had specific surface areas (SSAs) varies from 100 to 950 m<sup>2</sup> g<sup>-1</sup>. Considering the non-template method, tremendous progress has been made during the last years, with SSAs values impact of change to 1900 m<sup>2</sup> g<sup>-1</sup>[12], [13]. This character makes nucleophilic classes to target the B sites, while the N sites become sensitive to electrophilic groups. Several functional groups, which include hydroxyl (-OH) [14], amino (-NH<sub>2</sub>) [15], ether (-OR) [16], amine (-NHR)[15], aryl (-COR) [17], alkyl (-R) [18], and halogen (-X) [17]groups, and also some heteroatoms (C and O), were

being experimentally inserted into BN skeletons through chemical functional group addition.

Because of its optoelectronic characteristics and tunable band gap energy, BN is regarded a semiconductor, also because band gap of h-BN is relatively wide (varying from ~ 4.5 eV to 6 eV), it can only absorb light at wavelengths of < 275 nm in the electromagnetic light, which significantly limits its use of light[10], [19]. To improve the optical properties of BN, boron nitride is doped with a heteroatom. Doping leads to the atomic replacement, inside a BN 2D in-plane structure, of B or N atoms by heteroatoms without creating large regions produced of unaccompanied doping atoms. Implementation of particular heteroatoms to the Boron Nitride structures could bring about certain special features or substantial improvements of the pristine characteristic. Even though pure h-BN is a large band-gap photocatalyst, one significant approach to improving is to narrow its band gap energy while maintaining its initial honeycomb-like structure (i.e. the opposite approach to expanding the energy gap in graphene) to reach practical applications of photocatalyst. Even then, it is hard to find suitable elements in this area to be alloying elements with BN inside its own 2D hexagonal monolayer [7].

The absorption of a photon with energy equal to or greater than its band gap excites an electron to the conduction band (e<sub>CB</sub>), creating a hole in the valence band (h<sup>+</sup><sub>VB</sub>) in photocatalysis under UV or visible irradiation[2], [20-22]. The h<sup>+</sup><sub>VB</sub> can oxidize OH or water adsorbed at the surface to produce reactive oxygen species (ROS), primarily hydroxyl radicals (<sup>•</sup>OH), whereas the e<sub>CB</sub> can be scavenged by adsorbed molecular oxygen, resulting in the generation of superoxide radical anions (O<sub>2</sub><sup>•-</sup>). Singlet oxygen and hydrogen peroxide can be formed from O<sub>2</sub><sup>•-</sup>, with the latter yielding <sup>•</sup>OH as well [22]. Charge recombination at surface trapping sites or in the bulk of the photocatalyst competes with interfacial charge transfer from photogenerated electron/holes to acceptor/donor species at the surface. Nonradiative decay processes release heat as the electron/hole pair recombines, resulting in the loss of adsorbed photonic energy and the release of heat [20]. Several research evaluated the change in photodegradation rate in the presence of various scavengers to determine the key contributor in the photodegradation reaction [22]. The quantity of radicals generated under specific conditions is critical for elucidating the mechanism of degradation as well as assessing photocatalytic activity. Direct detection of these active species is rather difficult, due to their extremely high reactivity and short

lifetime ( $\text{HO}\cdot$ : 10–10 s [23];  $\text{O}_2\cdot^-$ : 51 s [24]). As a result, radical scavenger chemicals are commonly used to test them. Various analytical methods (UV/Vis, emission or ESR spectroscopy, chromatography or electrochemistry methods) can be employed to measure the concentration of the original compound or intermediates generated in the reaction of the scavenger and the radical [25].

## 2. Experimental

### 2.1. Instrumentation

The surface morphological properties, chemical composition, crystal quality, and structural properties of synthesized P-BN and Carbon Co-doped P-BN have been characterized and studied by utilizing the field-emission scanning electron microscopy (FE-SEM) (SEM 4500-Quanta), energy-dispersive X-ray (EDX) analysis, and analytical (XRD) X- Pert PRO (Cu  $K\alpha$  = 1.5406 Å at 40 kV, 30 mA) in the  $2\theta$  range of ( $20^\circ$  to  $70^\circ$ ) with the scanning rate of  $1^\circ/\text{min}$ . For monitoring photo-degradation process JENWAY 6700 and UV. -vis. Spectrophotometer type Perkin-Elmer lambda 25 has been used.

### 2.2. Chemicals

All chemicals used were of analytical grades and used as purchased without further treatments. 80% Phosphoric acid, Boric acid, sodium oxalate, potassium bromate were obtained from (Roth Company, Germany). Urea and Toluidine blue were bought from (labPak chemicals Ltd. UK), ammonia was purchased from (Merc Company, Germany). Isopropyl alcohol was purchased from (Fluka Ltd.) Ascorbic acid was bought from (Scharlau Germany).

### 2.3. Synthesis of phosphorous doped Boron nitride

For the synthesizing P-BN, boric acid (3 g) was dissolved in 50 mL deionized water then mixed with 15 mL of 25% ammonium solution coupled with the dropwise addition of 0.5 mL 85% phosphoric acid. The mixing was done using a magnetic stirrer and continued for half an hour then the solution was put in Teflon lined autoclave and placed in an oven for 24 hours at  $200^\circ\text{C}$ . The resulting solution was clear and no precipitate was observed and then the solvent was evaporated and the solid was dried in an oven at  $200^\circ\text{C}$  for two-hour to obtain white powder. After this stage, the powder was then examined in photo-degradation process and oxygen reactive species trapping experiments then it was characterized by SEM (scanning electron microscope),

EDX (energy dispersive x-ray), and XRD (X-ray diffraction) as shown in the following figures 2,3 and 4.

### 2.4. Synthesis of carbon co- doped phosphorous doped Boron nitride

For the synthesis of PC-BN, 3 grams of both urea and boric acid were mixed drop by drop in an aqueous solution, along with 1 mL 1M  $\text{H}_3\text{PO}_4$  drop by drop. The solution was mixed using a magnetic stirrer and continued for half an hour then the solution was put in Teflon lined autoclave and then placed in an oven for 24 hours at  $200^\circ\text{C}$ . The resulting solution was clear and then the solvent was evaporated and the solid was dried in an oven at  $200^\circ\text{C}$  for two hours until the white-like powder was obtained. After this stage, the powder was then examined in photo-degradation process and oxygen reactive species trapping experiments then it was characterized using SEM (scanning electron microscope), EDX (energy dispersive x-ray) and XRD (X-ray diffraction) as shown in the following Figs. 2, 3 and 4.

## 3. Results and Discussion

### 3.1. Theoretical modeling

The ab-initio calculations were performed by the plane-wave basis with the pseudopotential method in the framework of DFT, as implemented in the CASTEP cod material studio version 2017. We applied non-local functional generalized gradient approximations (GGA) [26]: Perdew-Burke-Ernzerhof (PBE) [27], [28] and hybrid functional was also applied including (Becke-3 Parameter-Lee-Yang-Parr) B3LYP [29] and (Heyd-Scuseria-Ernzerhof) exchange-correlation functional HSE06.

Each exchange-correlation (XC) functional was computed using kinetic energy cut-off: 500 eV at norm-conserving pseudopotentials. The Brillouin zone integration was performed using a  $4\times 4\times 4$  Monkhorst-Pack grid and the self-consistent field (SCF) tolerance was  $2\times 10^{-6}$  (eV/atom). The calculated lattice parameter and band gap values in (ev) were shown in **Tables 1** and **2** respectively. **Fig. 1** shows band structure and partial density of state for P-BN and CP-BN photo-catalysts. Hybrid functional B3LYP offered better results and consistency with the observed data. For the P-BN compound, the  $E_g$  is 3.698ev and 5.1ev as direct and indirect band gap, respectively while B3LYP, in the case of CP-BN, gives 2.6ev and 4.98ev as direct and indirect band gap respectively. Thus, this method was used to analyze the band structures and density of states.

The electronic partial density of states (PDOS) of P-BN and CP-BN materials was plotted in **Fig. 1**. It can be seen that the fermi level ( $E_F$ ) is near to the valence band (VB) in the case of P-BN while it is closer to the

conduction band in the case of CP-BN. The p-orbital showed a high DOS close to the  $E_F$  for both photo-catalysts.

**Table 1.** the calculated and experimental lattice parameters of P-BN and CP-BN

Photo-catalyst	a(Å)	b(Å)	c(Å)	V(Å <sup>3</sup> )	Alpha ( $\alpha$ )	Beta ( $\beta$ )	Gamma ( $\gamma$ )
P-BN	3.93	3.93	3.93	60.90	90°	90°	90°
CP-BN	3.88	3.88	3.88	58.38	92.02°	92.02°	92.02°

**Table 2.** The bandgap ( $E_g$ /eV) values of P-BN and CP-BN compounds utilizing norm conserving pseudopotentials.

Functional	P-BN		CP-BN	
	Direct band gap	Indirect band gap	Direct band gap	Indirect band gap
GGA (PBE)	1.892	3.3	1.6	3.867
HSE06	2.945	4.42	2.21	4.76
B3LYP	3.695	5.1	2.6	4.98
Experimental	4.21ev		4.16ev	

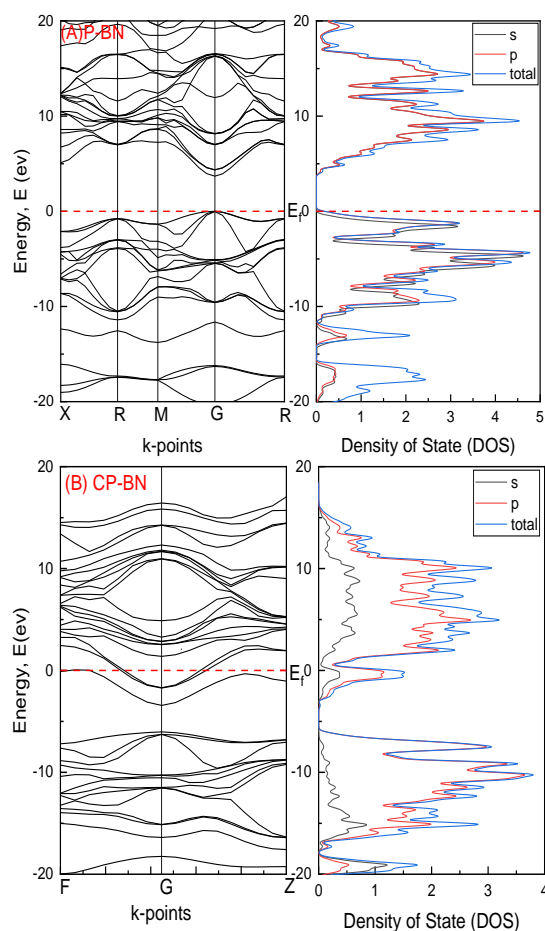


**Fig. 1.** The band structures of the (A)P-BN and (B)CP-BN compounds using B3LYP/norm conserving..

### 3.2. Characterization of the carbon and phosphorous doped boron nitride

#### 3.2.1. Phosphorous doped boron nitride

EDX results show the presence of only Boron, nitrogen and phosphorus for P-BN photocatalyst, it is worth mentioning that the presence of oxygen is due to the hydroxyl functionalized on the surface which makes nanoparticles soluble in water[7], [30]. In addition, the oxygen peak appears in both EDX charts as in **Fig. 3** below, this is due to the hydrophilic nature of the prepared photo-catalyst in which it functionalized hydroxyl group on its edge[16], [31-33] and it can easily absorb water vapor from the atmosphere and XRD proves that the only elements that are found in the crystal structure are Boron, Nitrogen and phosphorous. In the case of P-BN XRD, figure 8 shows that the peaks at  $2\theta$  equal to 41.9254 and 49.0290 and 72.5960 are at diffraction lines of 100, 102 and 104 respectively, which matches with boron nitride khl plans (h-BN) [11], [34-37]. From the XRD pattern, it can be investigated that all the diffraction peaks in all XRD patterns show the polycrystalline phase of BN doped with Phosphorus corresponded to the standard spectrum (JCPDS cards peak [ $^{\circ}2\theta$ .] at 41.9254, 49.0290 and 72.5960 match to No. 98-018-3793, 98-041-6155 and 98-016-7799 respectively for P-BN). These reference numbers prove the practical work. Considering elemental ratios, it has been recorded by EDX that the elemental ratio for P-BN was (B=63.75%, N=15.747%, P=5.856% and O=14.642%) as shown in **Fig. 4**.

#### 3.2.2. Phosphorous and carbon co-doped boron nitride

EDX results show the presence of only Boron, nitrogen, carbon and phosphorus in the case of carbon co-doped P-BN, it is worth mentioning that the presence of oxygen is due to the hydroxyl functionalized on the surface which makes nanoparticles soluble in water [7], [30]. However, the oxygen peak appears in both EDX charts as in figure 7, this is due to the hydrophilic nature of prepared photo-catalyst in which it functionalized hydroxyl group on its edge [16], [31-33] and it can easily absorb water vapor from the atmosphere and XRD prove that the only elements that are found in crystal structure are Boron, Nitrogen, carbon and phosphorous. In the case of carbon co-doped P-BN, the x-ray diffraction pattern gives the same results as in P-BN except two other peaks have appeared at  $2\theta$  equal to 27.2677 at diffraction line 002 [38] and 29.9290 which shows that the carbon has co-doped with phosphorous boron nitride and may due to the presence of graphitic like Boron nitride [6]. From the XRD pattern, it can investigate that all the diffraction peaks in all XRD patterns show the polycrystalline hexagonal phase of BN doped with carbon co-doped P-BN corresponded to the standard (JCPDS cards peak [ $^{\circ}2\theta$ ]) at 27.2677, 29.9290, 42.0609, 49.0565 and 72.6318 match to No. 98-018-3256, 98-024-6661, 98-018-3256, 98-024-6661 and 98-018-3256 respectively for CP-BN) this reference numbers proves the practical work. with respect to elemental ratios, it has been recorded by EDX that the elemental ratio CP-BN have (B=32.676%, N=18.514%, P=5.41%, O=13.533% and C=29.862%) as shown in Fig. 4.

Moreover, scherrer equation and Willimson-Hall (W-H) equations for crystallite size measurement that utilize XRD data have been applied to calculate the average particle size, it is found that the average particle size of CP-BN is roughly equal to 20.3 nm according to scherrer equation and 27.84 nm according to W-H equation. As regards to P-BN the crystallite size was 42.61nm when scherrer equation is applied and 16.83 nm in the case of W-H equation. Hence W-H equation is more suited for determining crystallite size because XRD peak broadening due to the strain has been taken into account in W-H equation as in the eq.1

$$\beta_{total} \cos\theta = \frac{K\lambda}{D} + 4\varepsilon \sin\theta \quad (1)$$

Where  $\varepsilon$  is macrostrain,  $\beta$  is the full width of the Bragg peak and half maximum (FWHM),  $\theta$  is peak angle,  $D$  is mean crystallite size and  $K \approx 1$  its value depends on the shape and geometry of the particle. In general, the width of a diffraction peak is affected by a number of factors, including inhomogeneous strain and crystal lattice imperfections (the most important factor), instrumental effects, dislocations, sub-boundaries, stacking faults, grain boundaries, twinning, micro stresses, coherency strain, chemical heterogeneities, and crystallite narrowness. Peak shift, peak broadening, and asymmetry, as well as anisotropic or other peak shape effects, are all caused by these causes [39-42].

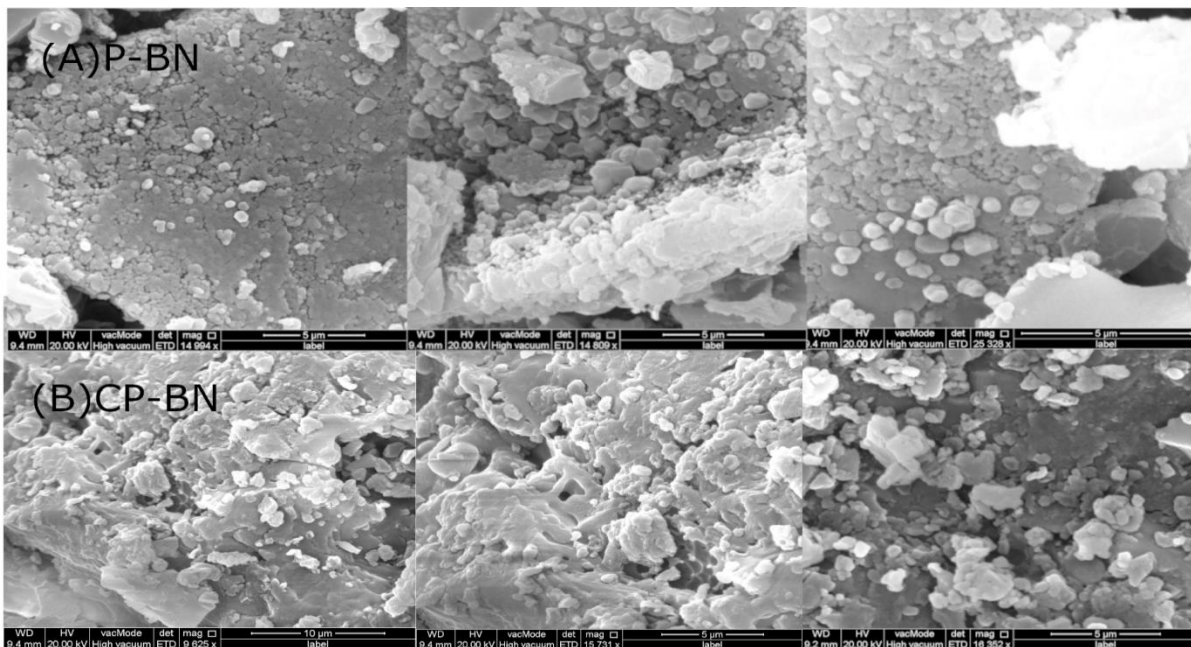
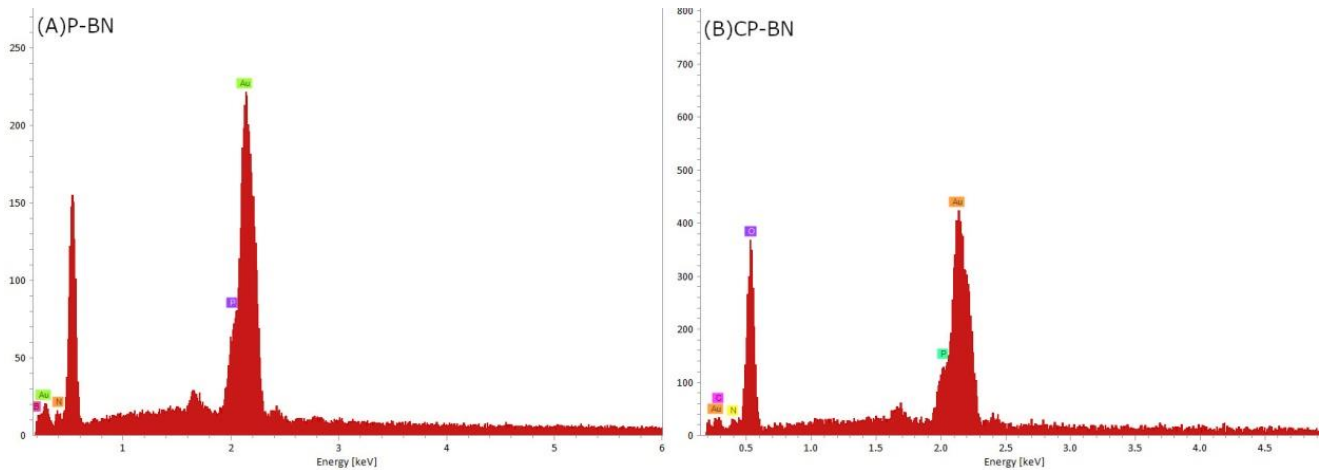
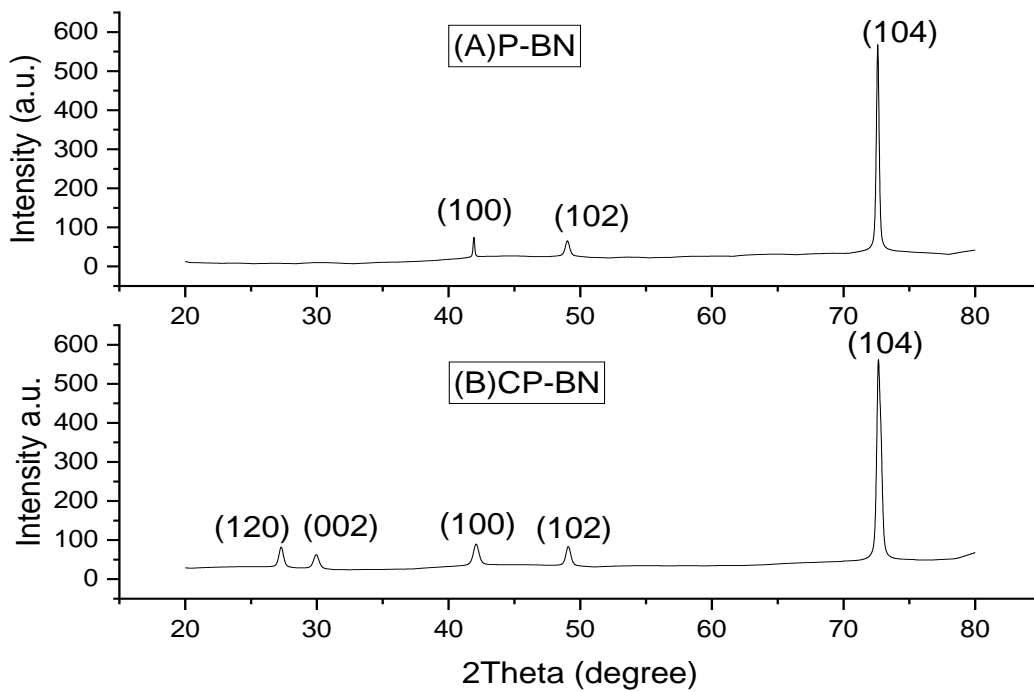


Fig. 2. Scanning electron microscopy (SEM) of (A) Phosphorous doped Boron Nitride P-BN and (B) Carbon and Phosphorus co-doped CP-BN.



**Fig. 3.** EDX data of (A) Phosphorous doped Boron Nitride P-BN and (B) Carbon and Phosphorus co-doped CP-BN.



**Fig. 4.** XRD peaks of (A) Phosphorous doped Boron Nitride P-BN and (B) Carbon and Phosphorus co-doped CP-BN.

Two peaks appear in XRD chart of CP-BN at 27.2677, 29.9290  $2\theta$ , while it does not exist in case of P-BN with some shifts at peak position, these shifts are related to the structural changes on the P-BN and CP-BN crystallite structure. As the dopant type change or concentration increases or decreases in crystallite size, depending on the nature of the peak shifting which is closely related to broadening or shrinking of the XRD peaks.

### 3.3. Photo-catalytic degradation

In this research, TB was used to investigate the photocatalytic activity of the prepared photocatalyst. In brief, 0.05 g of photocatalyst was mixed with 100 mL, 5 ppm of TB solution and then irradiated with ultraviolet (UV) water sterilization lamp 220v-240v 50/6 Hz (UVCD215 TS 6W). The degradation progress was monitored using spectrophotometer (JENWAY 6700 and UV. -vis. Spectrophotometer type Perkin-Elmer lambda 25).

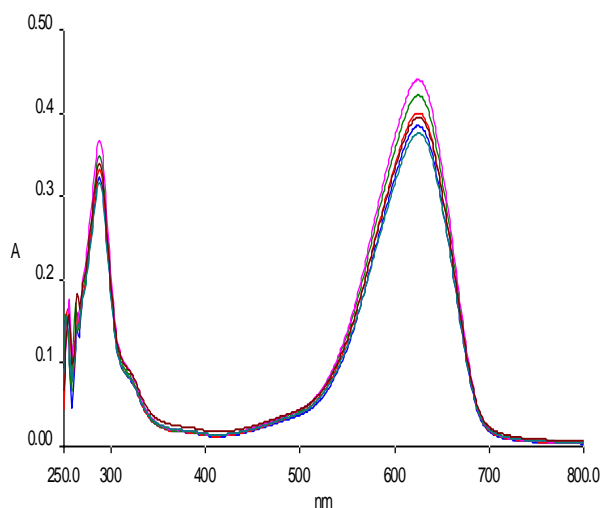
Because the gap energy  $E_g$  is 4.1, which is equivalent to 298.76 nm, the results reveal that both produced photocatalysts work in the ultraviolet range. Only radiation with wavelengths equal to or smaller than 298.76 nm

can initiate photodegradation. The degradation was carried out in basic, neutral, and acidic media, as well as in basic medium for both photo-catalysts, the degradation occurs better, as indicated in **Table 3**; and **Fig. 5** shows UV-vis. spectrum of photo-catalytic degradation concerning irradiation time:

Generally, It has been reported that the rate of photo-catalytic degradation changes with pH of solution. It is commonly accepted that in photocatalyst/aqueous systems, the potential of the surface charge is determined by the activity of ions (e.g. H<sup>+</sup> or pH). A convenient index of the tendency of a surface to become either positively or negatively charged as a function of pH is the value of the pH required to give zero net charge (pH ZPC)[43], [44]. pHZPC is a critical value for determining the sign and magnitude of the net charge carried on the photocatalyst surface during adsorption and photocatalytic degradation process. Most of the semiconductor oxides are amphoteric in nature, can associate eq.2 or dissociate eq.3 proton. To explain the relationship between the layer charge density and the adsorption, so-called models of surface complexation (SCM) was developed [45], [46], which consequently

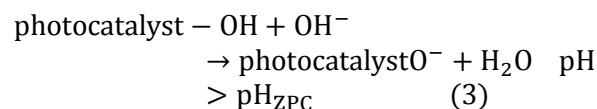
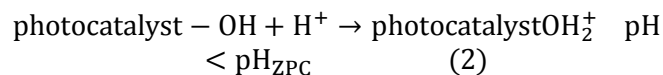
**Table 3.** Photo-catalytic performance of P-BN and carbon co-doped P-BN after one-hour irradiation of toluidine blue (TB) with UV light.

Photo-catalyst	% deg. Basic medium pH=9	% deg. Neutral medium pH=7	% deg. Acidic medium pH=3
P-BN	8.42	3.06	6.2
C P-BN	16	0.177	3.83



**Fig. 5.** UV-vis. Spectrum of photo-catalytic degradation of TB after one hour irradiation with UV light, 5ppm at pH 9.

affects the sorption-desorption processes and the separation and transfer of the photogenerated electron-hole pairs at the surface of the semiconductor particles. In the 2-pK approach we assume two reactions for surface protonation. The zero point charge pHZPC for ZnO is 9.0. For pH values lower than the pHZPC of ZnO, the surface becomes positively charged.



The resultant repulsive force between the adsorbate species and the adsorbent surface causes a comparatively weak adsorption in pH ranges where both the adsorbate species and the adsorbent surface have the same charge. In contrast, there are pH ranges in which the adsorbate species and adsorbent surface have opposite charges, generating an attraction force between the adsorbate and the surface (pHpzc > pKa for acids; pHpzc < pKa for bases). In certain pH ranges, these attraction forces, together with Van der Waals forces, create a maximum adsorption capacity [47].

In a study conducted by [46] the team on the photo-degradation of Congo Red catalyzed by ZnO, it was discovered that the rate constant varies with pH value and that the best results were obtained in basic medium.

Another study has been performed by [48] team on photochemical degradation of 4-chlorophenol using peroxy acetic acid (PAA) as a sensitizer, the result of this research shows that as the pH of solution altered the order of degradation changes as well, keeping the concentration and temperature constant basic, medium was slightly more efficient.

Various studies on toluidine blue dye have been conducted by various researchers, and it has been discovered that the efficacy of toluidine blue dye photocatalysis differs depending on the pH value. A study conducted by [49-51] found that the basic media was the best, whereas studies conducted by [3], [52], [53] also found that the acidic medium is the best. To summarize, the efficiency of a photocatalyst is determined by the pH of the medium. As previously said, the charge on the surface of the photocatalyst defines the optimal pH of solution.

### 3.4. Optical absorbance properties

To determine the band structure of the produced photocatalyst, UV-visible absorption spectra and reflectance were obtained, after which a Tauc and Kubelka-Munk plot was drawn, with the result agreeing with theoretical calculations as shown in **Fig. 6** [54-58]. It has been noted that the result of both equations was very close to each other given that 4.21eV and 4.27eV are for P-BN and 4.16 and 4.26 for CP-BN using Tauc and Kubelka-Munk equation respectively.

The photo Redox potential of produced nanostructured photocatalysts was determined as shown in **Table 2**. The valence band ( $E_{VB}$ ) and conduction band ( $E_{CB}$ ) potentials of the two materials may be approximated using the following Eq (4), (5) and (6)[59-64]:

$$E_{VB} = X - E_c + 0.5E_g \quad (4)$$

$$E_{CB} = X - E_c - 0.5E_g \quad (5)$$

$$E_{VB} = E_{CB} + E_g \quad (6)$$

In the above equation, the X and  $E_c$  are the absolute electronegativity of materials (defined as the arithmetic mean of the electron affinity and the first ionization of the constituent atoms) and energy of free electrons on the hydrogen scale ( $\sim 4.5$  eV), respectively. **Table 4** and **Fig. 7** show the redox potential energy of both photocatalysts at valence band  $E_{VB}$  and conduction band  $E_{CB}$  edges.

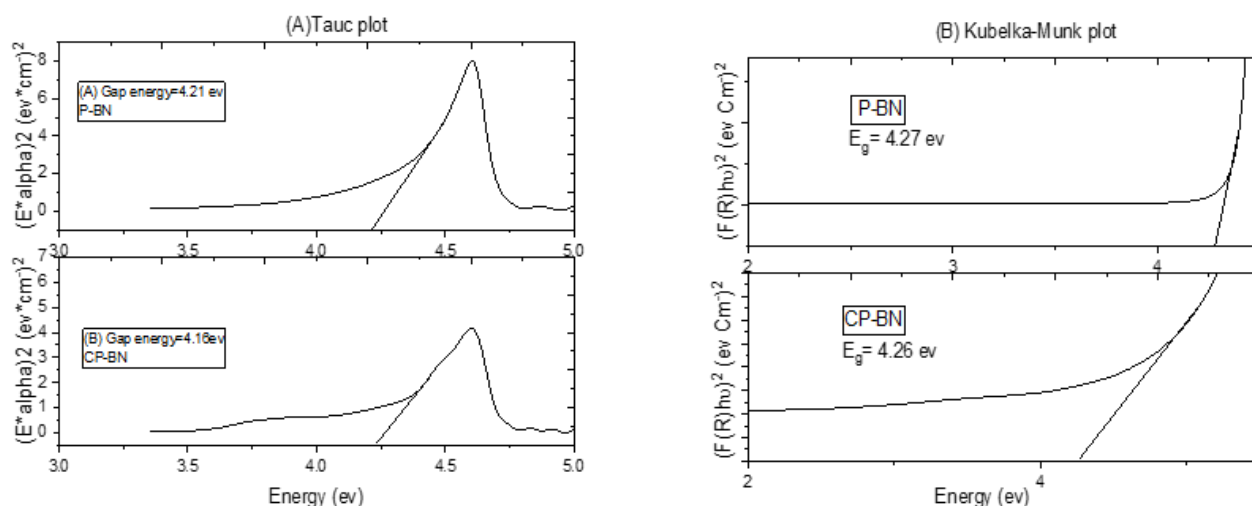


**Fig. 6.** Energy Band Gap ( $h\nu$ ) calculation of P-BN and carbon co-doped P-BN (A) Tauc plot ( $\alpha h\nu$ )<sup>2</sup> Versus and (B) Kubelka-Munk plot.

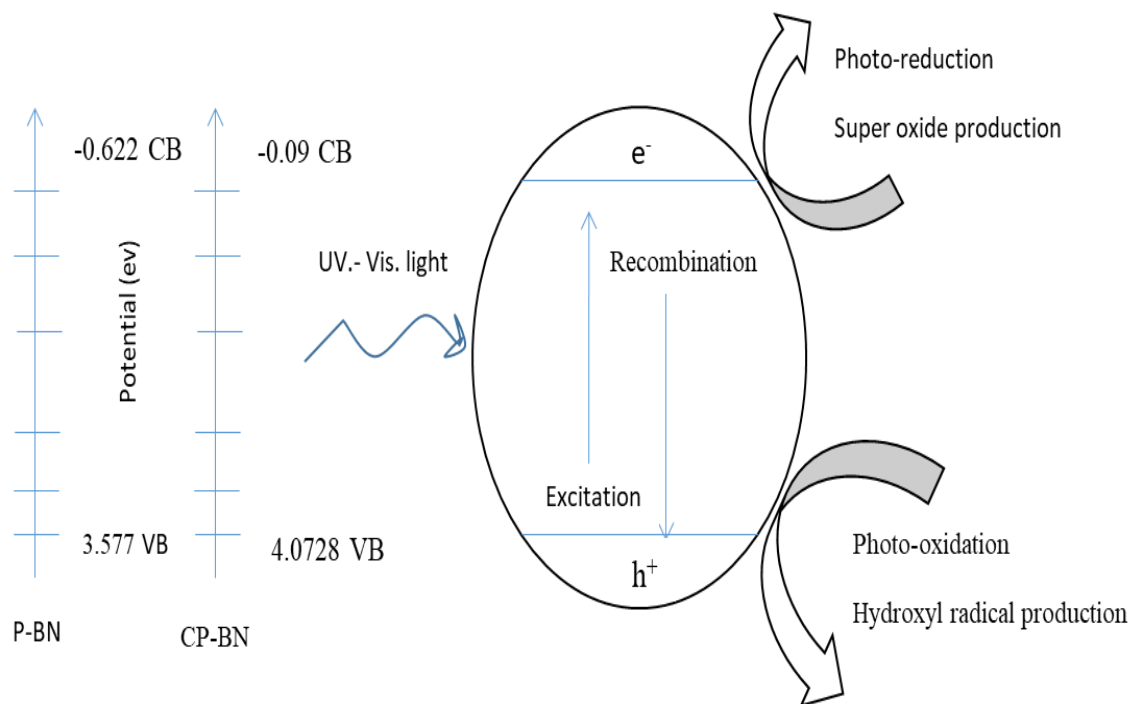
**Table 4.** valance band, conduction band and energy gap of both CP-BN and P-BN.

Photo-catalyst	$E_g$ (ev)	$E_{VB}$ (ev)	$E_{CB}$ (ev)
P-BN	4.223	3.577	-0.622
CP-BN	4.1618	4.0728	-0.09

### 3.5. Photocatalytic mechanism

Scavengers trapping experiments were performed to show and support theoretical calculations. In this experiment, Isopropyl alcohol (IPA), ascorbic acid, sodium oxalate, and potassium bromate were added to

determine the active species in degradation experiments as shown in **Fig. 8 (A)** and **(B)**. It has been shown by experiment that electron ( $e^-$ ) at conduction band which produces super oxide and hole ( $h^+$ ) at valance band which produces hydroxyl radical are both responsible and acting in the degradation process. However, sodium oxalate and potassium bromate scavenger trapping experiment shows the low efficiency of degradation that is due to rapid recombination of electron and hole [61], [65]. As it can be noticed from **Fig. 7** that trapping of  $e^-$  and  $h^+$  was very low, this tells that the recombination of excited electrons is very fast. For scavenger trapping experiments, 15 ppm of TB was mixed with 1mM of scavenger, then degradation proceeded as in the photocatalytic degradation part.



**Fig. 7.** Schematic diagram illustrates the principal mechanism of both photo-catalysts P-BN and CP-BN.

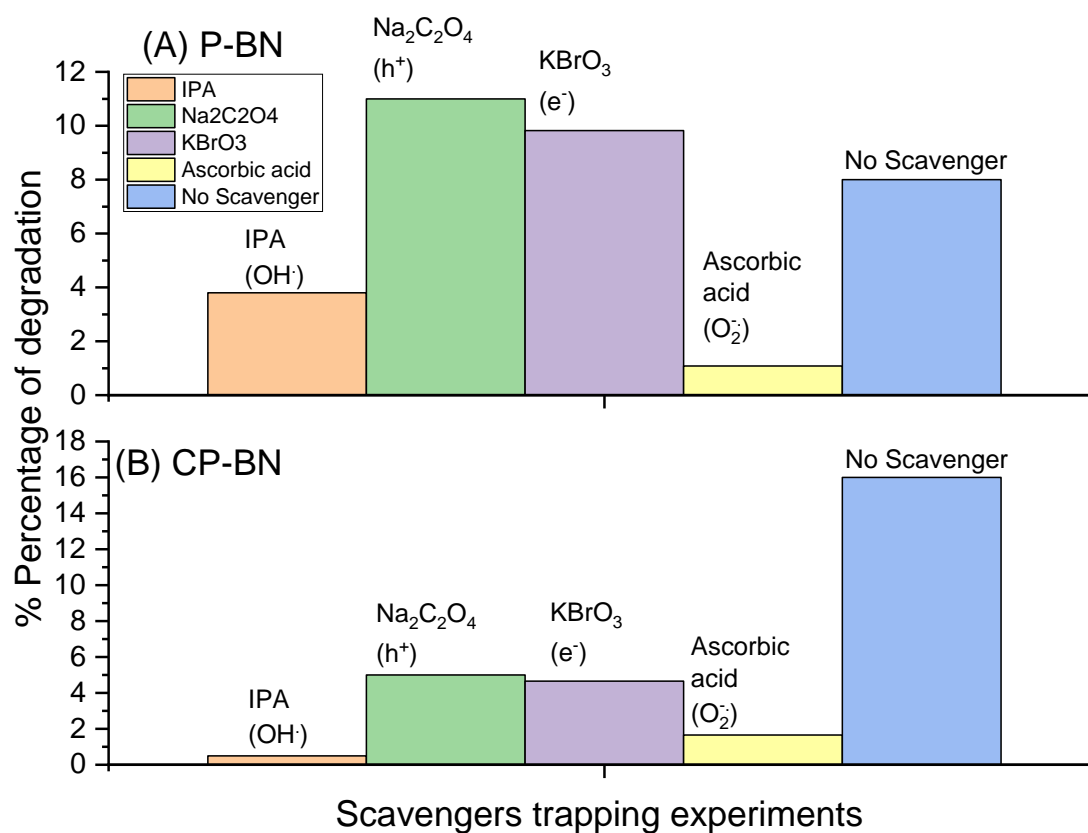


**Fig. 8.** Scavengers trapping experiments of active species in the photocatalytic reaction with 60 min UV. light irradiation in the presence of (A) P-BN and (B) CP-BN.

#### 4. Conclusions

Overall, phosphorous and carbon have been doped into boron nitride using two different chemicals: phosphoric acid, boric acid, and ammonia for P-BN and phosphoric acid, boric acid, and urea for CP-BN. Both photo-catalysts were UV. Light active. It has been shown from scavenger (trapping experiments) that both hydroxyl radical and super oxygen are found during the degradation process, but their efficiency is incompatible due to rapid charge recombination between electrons in the conduction band and holes in the valance band, as demonstrated by oxalate and bromate scavenging experiments. B3LYP and HSE06 hybrid functional coupled with GGA/PBE local functional were used in this work, it has been noted that the result given by B3LYP was closer to experimental data.

#### References

- [1] N. E. Fard and R. Fazaeli, "A Novel Kinetic Approach for Photocatalytic Degradation of Azo Dye with CdS and Ag/CdS Nanoparticles Fixed on a Cement Bed in a Continuous-Flow Photoreactor," *Int. J. Chem. Kinet.* 48 (11) (2016) 691–701.
- [2] M. M. Molla-Babaker and S. A. Idreesb, "Degradation of Congo Red Dye Using Homogeneous Photo Fenton Catalyst Coupled with Oxygen Kinetics and Statistical Analysis," *Asian J. Appl. Chem. Res.* 6 (1) (2020) 1–9.
- [3] H. A. M. Salim, S. A. Idrees, R. A. Rashid, A. A. Mohammed, S. M. Simo, and I. S. Khalo, "Photo-catalytic degradation of Toluidine Blue Dye in Aqueous Medium under Fluorescent Light," *ICOASE 2018 - Int. Conf. Adv. Sci. Eng.* (2018) 384–388.
- [4] S. A. Idrees, S. A. Naman, and A. Shorachi, "Kinetic and thermodynamic study of Trifluralin photo-degradation by ultra violet light," *IOP Conf. Ser. Mater. Sci. Eng.* 454 (1) (2018) 12–45.
- [5] A. S. Kasmaei, M. K. Rofouei, M. E. Olya, and S. Ahmed, "Kinetic and Thermodynamic Studies on the Reactivity of Hydroxyl Radicals in Wastewater Treatment by Advanced Oxidation Processes," *Prog. Color. Color. Coatings.* 13 (2019) 1–10.
- [6] T. Chen, Q. Zhang, Z. Xie, C. Tan, P. Chen, Y. Zeng, F. Wang, H. Liu, Y. Liu, G. Liu, and W. Lv, "Carbon nitride modified hexagonal boron nitride interface as highly efficient blue LED light-driven photocatalyst," *Appl. Catal. B Environ.* 238 (100) (2018) 410–421.
- [7] Q. Weng, X. Wang, X. Wang, Y. Bando, and D. Golberg, "Functionalized hexagonal boron nitride nanomaterials: Emerging properties and applications," *Chem. Soc. Rev.* 45 (14) (2016) 3989–4012.
- [8] R. T. Paine and C. K. Narula, "Synthetic Routes to Boron Nitride," *Chem. Rev.* 90 (1990) 73–91.
- [9] X. F. Jiang, Q. Weng, X. Bin Wang, X. Li, J. Zhang, D. Golberg, and Y. Bando, "Recent Progress on Fabrications and Applications of Boron Nitride Nanomaterials: A Review," *J. Mater. Sci. Technol.* 31 (6) (2015) 589–598.
- [10] J. Yu, L. Qin, Y. Hao, S. Kuang, X. Bai, Y. M. Chong, W. Zhang, and E. Wang, "Vertically aligned boron nitride nanosheets: Chemical vapor synthesis, ultraviolet light emission, and superhydrophobicity," *ACS Nano.* 4 (2010) 414–422.
- [11] B. Matović, J. Luković, M. Nikolić, B. Babić, N. Stanković, B. Jokić, and B. Jelenković, "Synthesis and characterization of nanocrystalline hexagonal boron nitride powders: XRD and luminescence properties," *Ceram. Int.* 42 (15) (2016) 16655–16658.
- [12] Q. Weng, X. Wang, C. Zhi, Y. Bando, and D. Golberg, "Boron nitride porous microbelts for hydrogen storage," *ACS Nano.* 7 (2) (2013) 1558–1565.
- [13] P. Wu, W. Zhu, Y. Chao, J. Zhang, P. Zhang, H. Zhu, C. Li, Z. Chen, H. Li, and S. Dai, "A template-free solvent-mediated synthesis of high surface area boron nitride nanosheets for aerobic oxidative desulfurization," *Chem. Commun.* 52 (2016) 144–147.
- [14] C. Y. Zhi, Y. Bando, T. Terao, C. C. Tang, H. Kuwahara, and D. Golberg, "Chemically activated boron nitride nanotubes," *Chem. - An Asian J.* 4 (10) (2009) 1536–1540.
- [15] T. Sainsbury, T. Ikuno, D. Okawa, D. Pacilé, J. M. J. Fréchet, and A. Zettl, "Self-assembly of gold nanoparticles at the surface of amine- and thiol-functionalized boron nitride nanotubes," *J. Phys. Chem. C*, vol. 111 (35) (2007) 12992–12999.
- [16] D. Kim, S. Nakajima, T. Sawada, M. Iwasaki, S. Kawauchi, C. Zhi, Y. Bando, D. Golberg, and T. Serizawa, "Sonication-assisted alcoholysis of boron nitride nanotubes for their sidewalls chemical peeling," *Chem. Commun.* 51 (33) (2015) 7104–7107.
- [17] D. Golberg, Y. Bando, C. Tang, and C. Zni, "Boron nitride nanotubes," *Adv. Mater.* 19 (18) (2007) 2413–2432.
- [18] F. Guo, J. Zhao, F. Li, D. Kong, H. Guo, X. Wang, H. Hu, L. Zong, and J. Xu, "Polar crystalline phases of PVDF induced by interaction with functionalized boron nitride nanosheets," *CrystEngComm.* 22 (37) (2020) 6207–6215.
- [19] Z. He, C. Kim, L. Lin, T. H. Jeon, S. Lin, X. Wang, and W. Choi, "Formation of heterostructures via direct growth CN on h-BN porous nanosheets for metal-free photocatalysis," *Nano Energy.* 42 (2017) 58–68.
- [20] M. Pelaez, P. Falaras, V. Likodimos, K. O'Shea, A. A. de la Cruz, P. S. M. Dunlop, J. A. Byrne, and D. D. Dionysiou, "Use of selected scavengers for the determination of NF-TiO<sub>2</sub> reactive oxygen species during the degradation of microcystin-LR under visible light irradiation," *J. Mol. Catal. A Chem.* 425 (2016) 183–189.
- [21] S. A. Idrees, R. N. Salih, K. Bashir, and A. A. Hamasaed, "Kinetic Study of Congo-Red Photocatalytic Degradation in Aqueous Media Using Zinc Oxide as Photo Catalyst Under Led Light," *Sci. J. Univ. Zakho.* 9 (2021) 20–24.
- [22] M. R. Hoffmann, S. T. Martin, W. Choi, and D. W. Bahnemann, "Environmental Applications of

- Semiconductor Photocatalysis,” *Chem. Rev.* 95 ( 1995) 69–96.
- [23] P. Fernández-Castro, M. Vallejo, M. F. San Román, and I. Ortiz, “Insight on the fundamentals of advanced oxidation processes: Role and review of the determination methods of reactive oxygen species,” *J. Chem. Technol. Biotechnol.* 90 (5) ( 2015) 796–820.
- [24] B. G. Kwon, J.-O. Kim, and J.-K. Kwon, “An Advanced Kinetic Method for HO<sub>2</sub>·/O<sub>2</sub>·- Determination by Using Terephthalate in the Aqueous Solution,” *Environ. Eng. Res.* 17 (4) ( 2012) 205–210.
- [25] O. Fónagy, E. Szabó-Bárdos, and O. Horváth, “1,4-Benzoquinone and 1,4-hydroquinone based determination of electron and superoxide radical formed in heterogeneous photocatalytic systems,” *J. Photochem. Photobiol. A Chem.* 407 (2021).
- [26] W. KOHN and L. J. SHAM, “Self-Consistent Equations Including Exchange and Correlation Effects,” *Phys. Rev.* 140 (4A) ( 1965) A1133–A1137.
- [27] J. P. Perdew, K. Burke, and M. Ernzerhof, “Generalized gradient approximation made simple,” *Phys. Rev. Lett.*, vol. 77, no. 18, pp. 3865–3868, 1996, doi: 10.1103/PhysRevLett.77.3865.
- [28] M. K. Abdel-Sattar and M. Taha, “Electronic structures and optoelectronic properties of ATiOPO<sub>4</sub> (A = H, Li, Na, K, Rb, Cs, Fr, NH<sub>4</sub>, Ag) compounds and their applications in water splitting, CO<sub>2</sub> reduction, and photodegradation,” *Mater. Res. Express.* 7 (4) 2020.
- [29] R. G. P. Chengteh Lee, Weitao Yang, “Development of the Colle-Salvetti correlation-energy formula into a functional of the electron density,” *Phys. Rev. B.* 37 (2) ( 1988) 785–789.
- [30] X. Shi, K. Wang, J. Tian, X. Yin, B. Guo, G. Xi, W. Wang, and W. Wu, “Few-Layer Hydroxyl-Functionalized Boron Nitride Nanosheets for Nanoscale Thermal Management,” *ACS Appl. Nano Mater.* 3 (3) (2020) 2310–2321.
- [31] Y. Zhan, J. Yang, L. Guo, F. Luo, B. Qiu, G. Hong, and Z. Lin, “Targets regulated formation of boron nitride quantum dots – Gold nanoparticles nanocomposites for ultrasensitive detection of acetylcholinesterase activity and its inhibitors,” *Sensors Actuators, B Chem.* 279 ( 2019) 61–68.
- [32] S. Angizi, F. Shayeganfar, M. H. Azar, and A. Simchi, “Surface/edge functionalized boron nitride quantum dots: Spectroscopic fingerprint of bandgap modification by chemical functionalization,” *Ceram. Int.* 46 ( 2020) 978–985.
- [33] J. H. Jung, M. Kotal, M. H. Jang, J. Lee, Y. H. Cho, W. J. Kim, and I. K. Oh, “Defect engineering route to boron nitride quantum dots and edge-hydroxylated functionalization for bio-imaging,” *RSC Adv.* 6 (77) ( 2016) 73939–73946.
- [34] C. Huang, C. Chen, X. Ye, W. Ye, J. Hu, C. Xu, and X. Qiu, “Stable colloidal boron nitride nanosheet dispersion and its potential application in catalysis,” *J. Mater. Chem. A.* 1 (39) ( 2013) 12192–12197.
- [35] Ö. Şen, M. Emanet, and M. Çulha, “One-step synthesis of hexagonal boron nitrides, their crystallinity and biodegradation,” *Front. Bioeng. Biotechnol.* 9 ( 2018) 1–9.
- [36] T. A. Baeraky, Y. H. Afandi, and H. A. Al-Jawhari, “The influence of microwave frequencies at high temperatures on structural properties of h-BN,” 11 (2011) 63-67.
- [37] R. N. Muthu, S. Rajashabala, and R. Kannan, “Hydrogen storage performance of lithium borohydride decorated activated hexagonal boron nitride nanocomposite for fuel cell applications,” *Int. J. Hydrogen Energy.* 42 (23) (2017) 15586–15596.
- [38] J. Xiong, W. Zhu, H. Li, L. Yang, Y. Chao, P. Wu, S. Xun, W. Jiang, M. Zhang, and H. Li, “Carbon-doped porous boron nitride: Metal-free adsorbents for sulfur removal from fuels,” *J. Mater. Chem. A.* 3 (24) ( 2015) 12738–12747.
- [39] S. D. Khairnar, M. R. Patil, and V. S. Shrivastava, “Hydrothermally synthesized nanocrystalline Nb<sub>2</sub>O<sub>5</sub> and its visible-light photocatalytic activity for the degradation of congo red and methylene blue,” *Iran. J. Catal. Hydrothermally.* 2 (8) ( 2018) 143–150.
- [40] A. Yousefi and A. NezamzadehEjehieh, “Preparation and characterization of SnO<sub>2</sub>-BiVO<sub>4</sub>-CuO catalyst and kinetics of phenazopyridine photodegradation,” *Iran. J. Catal. Prep.* 11 (3) (2021) 247–259.
- [41] A. F. Abdulrahman, S. M. Ahmed, N. M. Ahmed, and M. A. Almessiere, “Fabrication, characterization of ZnO nanorods on the flexible substrate (Kapton tape) via chemical bath deposition for UV photodetector applications,” *AIP Conf. Proc.* 1875 (2017) 0200041-0200046.
- [42] A. F. Abdulrahman, S. M. Ahmed, N. M. Ahmed, and M. A. Almessiere, “Different substrates effects on the topography and the structure of the ZnO nanorods grown by chemical bath deposition method,” *Dig. J. Nanomater. Biostructures.* 11 (3) (2016) 1007–1016.
- [43] F. Zhang, J. Zhao, T. Shen, H. Hidaka, E. Pelizzetti, and N. Serpone, “TiO<sub>2</sub>-assisted photodegradation of dye pollutants II. Adsorption and degradation kinetics of eosin in TiO<sub>2</sub> dispersions under visible light irradiation,” *Appl. Catal. B Environ.* 15 ( 1998) 147–156.
- [44] D. E. Yates, S. Levine, and T. W. Healy, “Site-binding model of the electrical double layer at the oxide/water interface,” *J. Chem. Soc. Faraday Trans. 1 Phys. Chem. Condens. Phases.* 70 (1974) 1807–1818.
- [45] J. Fernández, J. Kiwi, C. Lizama, J. Freer, J. Baeza, and H. D. Mansilla, “Factorial experimental design of Orange II photocatalytic discoloration,” *J. Photochem. Photobiol. A Chem.* 151 ( 2002) 213–219.
- [46] L. Nadjia, E. Abdelkader, and B. Ahmed, “Photodegradation study of Congo Red in Aqueous Solution using ZnO/ UV-A: Effect of pH And Band Gap of other Semiconductor Groups,” *J. Chem. Eng. Process Technol.* 02 (02) (2011) 1–7.
- [47] S. Ghattavi and A. Nezamzadeh-Ejehieh, “A brief study on the boosted photocatalytic activity of AgI/WO<sub>3</sub>/ZnO in the degradation of methylene blue under visible light irradiation,” *Desalin. Water Treat.* 166 (2019) 92–104.

- [48] M. Mukhopadhyay and D. P. Daswat, "Kinetic and mechanistic study of photochemical degradation of 4-chlorophenol using peroxy acetic acid (PAA)," *Desalin. Water Treat.* 52 (28–30) (2014) 5704–5714.
- [49] P. Parsoya and S. C. Ameta, "Use of Zinc Ferrite as Photocatalyst for Degradation of Toluidine Blue," *J. Curr. Chem. Pharm. Sci.* 6 (4) (2016) 63–69.
- [50] B. Pare, V. Joshi, and S. Piplode, "EFFECT OF OPERATIONAL PARAMETERS ON PHOTOCATALYTIC DEGRADATION OF TOLUIDINE BLUE UTILIZING BiOCl NANOPATES IN SOLAR LIGHT," *Int. J. Eng. Technol. Manag. Res.* 4 (12) (2020) 43–54.
- [51] R. Ameta, S. Sharma, S. Sharma, and Y. Gorana, "Visible Light Induced Photocatalytic Degradation of Toluidine Blue-O by using Molybdenum Doped Titanium Dioxide," *Eur. J. Adv. Eng. Technol.* 2 (8) (2015) 95–99.
- [52] H. Mohammad Salim and S. Mohammad Salih, "Photodegradation Study of Toluidine Blue Dye in Aqueous Solution using Magnesium Oxide as a Photocatalyst," *Int. J. Chem.* 7 (2) (2015) 143.
- [53] S. Dhahir, "Removal Color Study of Toluidine Blue dye from Aqueous Solution by using Photo-Fenton Oxidation," *Baghdad Sci. J.* 13 (2) (2016) 440–446.
- [54] R. Mohammed, S. Ahmed, A. Abdulrahman, and S. Hamad, "Synthesis and Characterizations of ZnO Thin Films Grown by Physical Vapor Deposition Technique," *J. Appl. Sci. Technol. Trends.* 1 (4) (2020) 135–139.
- [55] A. F. Abdulrahman, S. M. Ahmed, and M. A. Almessiere, "Effect of the growth time on the optical properties of ZnO nanorods grown by low temperature method," *Dig. J. Nanomater. Biostructures.* 12 (4) (2017) 1001–1009.
- [56] B. Manikandana, K. R. John, and M. Rita, "Optical, Morphological and Microstructural Investigation of TiO<sub>2</sub> nanoparticles for Photocatalytic application," *Iran. J. Catal.* 1 (11) (2021) 1–11.
- [57] S. Jafari and A. Nezamzadeh-Ejhieh, "Supporting of coupled silver halides onto clinoptilolite nanoparticles as simple method for increasing their photocatalytic activity in heterogeneous photodegradation of mixture of 4-methoxy aniline and 4-chloro-3-nitro aniline," *J. Colloid Interface Sci.* 490 (2017) 478–487.
- [58] Z. Khodami and A. Nezamzadeh-Ejhieh, "Investigation of photocatalytic effect of ZnO-SnO<sub>2</sub>/nano clinoptilolite system in the photodegradation of aqueous mixture of 4-methylbenzoic acid/2-chloro-5-nitrobenzoic acid," *J. Mol. Catal. A Chem.* 409 (3) (2015) 59–68.
- [59] A. Habibi-yangjeh and M. Shekofteh-gohari, "Novel magnetic Fe<sub>3</sub>O<sub>4</sub> / ZnO / NiWO<sub>4</sub> nanocomposites : Enhanced visible-light photocatalytic performance through p-n heterojunctions," *Sep. Purif. Technol.* 184 (2017) 334–346.
- [60] M. Mousavi, A. Habibi-yangjeh, and M. Abitorabi, "Fabrication of novel magnetically separable nanocomposites using graphitic carbon nitride , silver phosphate and silver chloride and their applications in photocatalytic removal of different pollutants using visibl," *J. Colloid Interface Sci.* 480 (2016) 218–231.
- [61] M. Pirhashemi and A. Habibi-Yangjeh, "Ultrasonic-assisted preparation of plasmonic ZnO/Ag/Ag<sub>2</sub>WO<sub>4</sub> nanocomposites with high visible-light photocatalytic performance for degradation of organic pollutants," *J. Colloid Interface Sci.* 491 (2016) 216–229.
- [62] H. Dong, G. Chen, J. Sun, C. Li, Y. Hu, and C. Lv, "An advanced Ag-based photocatalyst Ag<sub>2</sub>Ta<sub>4</sub>O<sub>11</sub> with outstanding activity," *Phys. Chem. Chem. Phys.* 16 (2014) 23915–23921.
- [63] S. Brook, "The absolute energy positions of conduction and valence bands of selected semiconducting minerals," *Am. Mineral.* 85 (2000) 543–556.
- [64] L. Dia, H. Yanga, T. Xian, and X. Chen, "Enhanced Photocatalytic Degradation Activity of BiFeO<sub>3</sub> Microspheres by Decoration with g-C<sub>3</sub> N<sub>4</sub> Nanoparticles," *Materials Research.* 21 (5) (2018) 1–10.
- [65] P. Ju, P. Wang, B. Li, H. Fan, S. Ai, D. Zhang, and Y. Wang, "A novel calcined Bi<sub>2</sub>WO<sub>6</sub>/BiVO<sub>4</sub> heterojunction photocatalyst with highly enhanced photocatalytic activity," *Chem. Eng. J.* 236 (15) (2014) 430–437.